# Research Advances in the Synthesis of Nanocarbon−Based Photocatalysts and Their Applications for Photocatalytic Conversion of Carbon Dioxide to Hydrocarbon Fuels

**ARTICLE** *in* ENERGY & FUELS · OCTOBER 2013

Impact Factor: 2.79 · DOI: 10.1021/ef401426x



**2 AUTHORS:**

Hongqi Sun
Curtin University
**88** PUBLICATIONS **2,092** CITATIONS
SEE PROFILE

Shaobin Wang
Curtin University
**271** PUBLICATIONS **9,327** CITATIONS
SEE PROFILE

energy&fuels

Review

pubs.acs.org/EF

# Research Advances in the Synthesis of Nanocarbon-Based Photocatalysts and Their Applications for Photocatalytic Conversion of Carbon Dioxide to Hydrocarbon Fuels

Hongqi Sun* and Shaobin Wang*

Department of Chemical Engineering, Curtin University, GPO Box U1987, Perth, Western Australia 6845, Australia

**ABSTRACT:** Hydrocarbon fuels are the most important sources of energy in modern society because of their natural abundance, stability, and high energy density. However, the emissions of carbon dioxide from them and the associated global warming effect impose worldwide pressure on the use of sustainable solar energy and carbon dioxide transformation and sequestration. Photocatalytic conversion of $CO_2$ to fuels using semiconductors is proposed as an effective solution. More recently, nanocarbons, such as carbon nanotube, graphene oxide, and graphene, possessing high thermal conductivity, high theoretical specific surface area, unique carrier mobility, low-dimensional structure, and $sp^2$-hybridized carbon configuration, have shown promotion to photocatalysis. It has been proven that nanocarbon/semiconductor hybrids can be a competitive material compared to traditional metal oxides for $CO_2$ reduction. This review summarizes the recent research advances in the synthesis of nanocarbon hybrid photocatalysts and their applications in photocatalytic reduction of $CO_2$ to hydrocarbons. The roles of nanocarbons in extending light absorption, increasing separation of carriers, band gap engineering, and preferred $CO_2$ adsorption in manipulating activity/selectivity are discussed. The studies in this topic will facilitate the design of advanced functional materials for energy innovation via solar energy use.

## 1. INTRODUCTION

The development of industry and society heavily relies on energy consumption, which is estimated to increase to 27 TW by 2050 and may reach 43 TW by 2100, as compared to the current level of 15 TW. Solar energy is an abundant, clean, and sustainable energy resource, providing about 120 000 TW annually to the Earth.[1] On the other hand, as the currently most important energy contributor, fossil fuels are depleting and they produce carbon dioxide, with the emissions continuously increasing the atmospheric $CO_2$ level. $CO_2$ is one of the major greenhouse gases and plays a significant role in global warming. Therefore, simultaneous $CO_2$ reduction and solar energy conversion would be a fascinating solution to the above barriers to the sustainable development of industry and economy.

In $CO_2$ reduction and transformation, photocatalytic conversion of $CO_2$ to fuels, such as $CH_4$, $CH_3OH$, and CO, has demonstrated its effectiveness for the pursuit of "solar fuel".[2,3] A pioneering study was reported in 1979, when Inoue et al.[4] observed the conversion of $CO_2$ to small amounts of HCOOH, HCHO, $CH_3OH$, and $CH_4$ over semiconductor photocatalysts, such as $TiO_2$, ZnO, CdS, GaP, SiC, and $WO_3$, suspended in water solution under ultraviolet (UV) irradiations. In photoreduction of $CO_2$ to fuels, various surface reactions will take place and the processes of multiple electron/proton transfers associated with a variety of final products are listed below.[5]

$$H_2O + 2h^+ \rightarrow 1/2O_2 + 2H^+ \qquad E^\circ_{redox}\ (V)\ \text{versus NHE} = 0.82 \tag{1}$$

$$2H^+ + 2e^- \rightarrow H_2 \qquad E^\circ_{redox}\ (V)\ \text{versus NHE} = -0.41 \tag{2}$$

$$CO_2 + 2H^+ + 2e^- \rightarrow CO + H_2O \qquad E^\circ_{redox}\ (V)\ \text{versus NHE} = -0.53 \tag{3}$$

$$CO_2 + 2H^+ + 2e^- \rightarrow HCO_2H \qquad E^\circ_{redox}\ (V)\ \text{versus NHE} = -0.43 \tag{4}$$

$$CO_2 + 4H^+ + 4e^- \rightarrow CH_2O + H_2O \qquad E^\circ_{redox}\ (V)\ \text{versus NHE} = -0.48 \tag{5}$$

$$CO_2 + 6H^+ + 6e^- \rightarrow CH_3OH + H_2O \qquad E^\circ_{redox}\ (V)\ \text{versus NHE} = -0.32 \tag{6}$$

$$CO_2 + 8H^+ + 8e^- \rightarrow CH_4 + 2H_2O \qquad E^\circ_{redox}\ (V)\ \text{versus NHE} = -0.244 \tag{7}$$

The gas products may include CO, $CH_4$, and $H_2$ (via water splitting), and the liquid hydrocarbons may have HCOOH, $CH_2O$, and $CH_3OH$. The involved redox potentials for $H^+/H_2$, $CO_2/CO$, $CO_2/CH_4$, $CO_2/CH_3OH$, and $CO_2/HCOOH$ are 0, −0.11, −0.244, −0.32, and −0.43 V (NHE, pH 7), respectively.[6] The selectivity was suggested to be strongly dependent upon the redox potentials of photoinduced carriers, which are controlled by the band edge positions of the photocatalysts.[2,4] It was

**Special Issue:** 4th (2013) Sino-Australian Symposium on Advanced Coal and Biomass Utilisation Technologies

**Received:** July 24, 2013
**Revised:** October 8, 2013
**Published:** October 14, 2013

   dx.doi.org/10.1021/ef401426x | *Energy Fuels* 2014, 28, 22−36

concluded that the photocatalyst materials act the predominant role in photocatalytic reduction of $CO_2$ to fuels. A competitive photocatalyst needs to fulfill three requirements, e.g., wide absorption to solar spectra (band gap energy), appropriate redox potential (band edges), and specific selectivity.

In previous studies, wide band gap semiconductors are usually applied as photocatalysts, such as $TiO_2$, $WO_3$, GaP, ZnO, and SiC, to ensure the appropriate conduction band position for photoreduction of $CO_2$.[7−9] However, these photocatalysts can only use the UV section (less than 5%) of solar spectrum energy. To enhance the photocatalytic activity and improve the solar energy use, a variety of modification methods have been employed. Liu et al.[5] reviewed the engineering band gap of $TiO_2$ nanomaterials for light harvesting in solar energy production, such as metal doping (Rh, Pd, Cu, Ag, Fe, Cr, etc.), surface sensitization, semiconductor coupling, and immobilization. Garcia et al.[10] summarized the research advances in photocatalytic $CO_2$ reduction by pure $TiO_2$ as well as metal- and nonmetal-doped titania, noble metals supported on titania, and micro-/mesoporous titanosilicates or porous matrices containing titania clusters. Anpo et al.[11] reported the research progress in photocatalytic reduction of $CO_2$ with $H_2O$ on systems of small-particle $TiO_2$, metal-loaded $TiO_2$, $TiO_2$ single crystals, Ti-oxide anchored on zeolite, Ti-containing zeolite and mesoporous molecular sieves, Ti-oxide anchored on porous silica glass, Ti-containing porous silica film, and Ti/Si binary oxide. Navalon et al.[12] recently summarized the photocatalytic $CO_2$ reduction using non-titanium metal oxides and sulfides. For visible-light photocatalysis, the metal oxides include $BiVO_4$, $Bi_2WO_6$, $WO_3$, $InTaO_4$, $NaNbO_3$, $Zn_2GeO_4$, $ZnGa_2O_4$, $ZnAl_2O_4$, $Cu_2O$, etc., while metal sulfides as visible-light photocatalysts for $CO_2$ reduction include $Bi_2S_3$, CdS, $Bi_2S_3$/CdS, ZnS, $Cu_xAg_yIn_zZn_kS_m$, etc.

More recently, nanocarbons, such as fullerene,[13] nanodiamond,[14] carbon nanotube (CNT),[15] and graphene oxide (GO)/graphene,[16,17] have demonstrated their promising functions as promoters or catalysts for photocatalysis. Extensive studies have applied CNT, graphene, and GO for enhanced production of solar fuels. Multi-walled carbon nanotube (MWCNT)-supported $TiO_2$ photocatalysts were prepared by different methods. The composites prepared by sol−gel methods would lead to the main product of $C_2H_5OH$, while HCOOH was found to be formed on photocatalysts from a hydrothermal method.[18] The unique electronic and optical properties of graphene also make it as a promising candidate for functionalizing and tailoring $TiO_2$ photocatalytic performance. Hersam et al.[19] reported that the nanocomposites of graphene−$TiO_2$ based on the less defective solvent-exfoliated graphene exhibited a significant enhancement in $CO_2$ photocatalytic reduction. GO was recently demonstrated as a promising photocatalyst for conversion of $CO_2$ to methanol by photocatalysis.[20]

It was found that nanocarbons have played versatile roles in photocatalytic conversion of $CO_2$ to hydrocarbons; however, only few reviews mentioned the functions of the nanocarbons in such a process.[6,21] Therefore, a comprehensive review on the research advances of nanocarbon hybrid photocatalysts for visible-light photocatalytic conversion of $CO_2$ to hydrocarbons and the functions of nanocarbons in the system will be highly valuable for understanding of composite structure and designing highly efficient photocatalyst materials for solar fuel production from $CO_2$. In this paper, we will discuss the synthesis of different nanocarbon-based photocatalysts, their performance in $CO_2$ conversion, and the roles of nanostructured carbons in the photocatalytic $CO_2$ reduction.

## 2. SYNTHESIS OF NANOCARBON HYBRID PHOTOCATALYSTS

**2.1. Nanocarbon−$TiO_2$ Hybrids.** Because $TiO_2$ is a widely used semiconductor and highly effective photocatalyst for photoreaction, most researchers focused on its modification and application. Sol−gel and hydrothermal methods have been widely employed to prepare CNT−$TiO_2$ hybrid photocatalysts.[15] Puma et al.[22] prepared CNT/$TiO_2$ core−shell nanocomposites by a surfactant wrapping sol−gel method. Figure 1 schematically

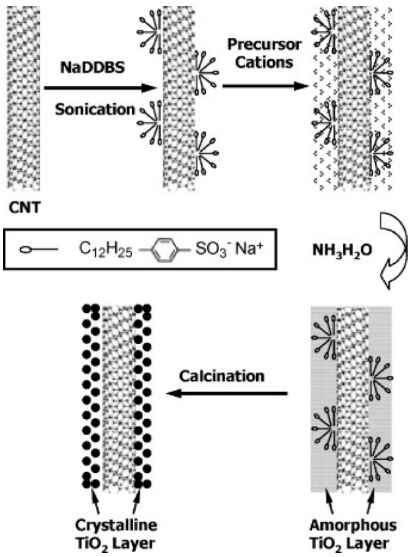


**Figure 1.** Preparation of CNTs/$TiO_2$ nanocomposites by the surfactant wrapping sol−gel method, in the presence of sodium dodecylbenzesulfonate (NaDDBS).[22]

shows the preparation procedure of CNTs/$TiO_2$ nanocomposites. Different titania precursors, such as titanium ethoxide, titanium isopropoxide, and titanium butoxide were used. In this method, a uniform and well-defined nanoscale $TiO_2$ layer on CNTs was fabricated and produced a mesoporous nanocomposite film.

CNT/$TiO_2$ sphere composite photocatalysts were synthesized by a facile one-step hydrothermal method using titanium tetrafluoride.[23] A given amount of purified MWCNTs was first dispersed in $TiF_4$ solution with different concentrations, and then the mixed solution underwent a hydrothermal reaction at certain conditions. Figure 2 shows the morphologies of the samples from different conditions. It was found that $TiO_2$ spheres were well-wrapped around by the MWCNTs. Moreover, the structure of MWCNTs in the composites remained unchanged after the hydrothermal synthesis. Cong et al.[24] reported the preparation of carbon-doped $TiO_2$ coating on MWCNTs by oxidation of TiC on MWCNTs. By precise control of the oxidation temperature, the $TiO_2$ coating can closely contact with MWCNTs via chemical bonds for efficient charge transfer and adsorption of reactants. Wond et al.[25] reported that ultrasonic irradiation can be used for preparation of $TiO_2$/CNT composites, in which CNTs are covered by $TiO_2$ through the formation of an ester-like linkage and there are more hydroxyl groups on the surface of the composites.

A large variety of methods have been developed for preparation of graphene/$TiO_2$ composites. Jiao et al.[26] reported a


dx.doi.org/10.1021/ef401426x | Energy Fuels 2014, 28, 22−36

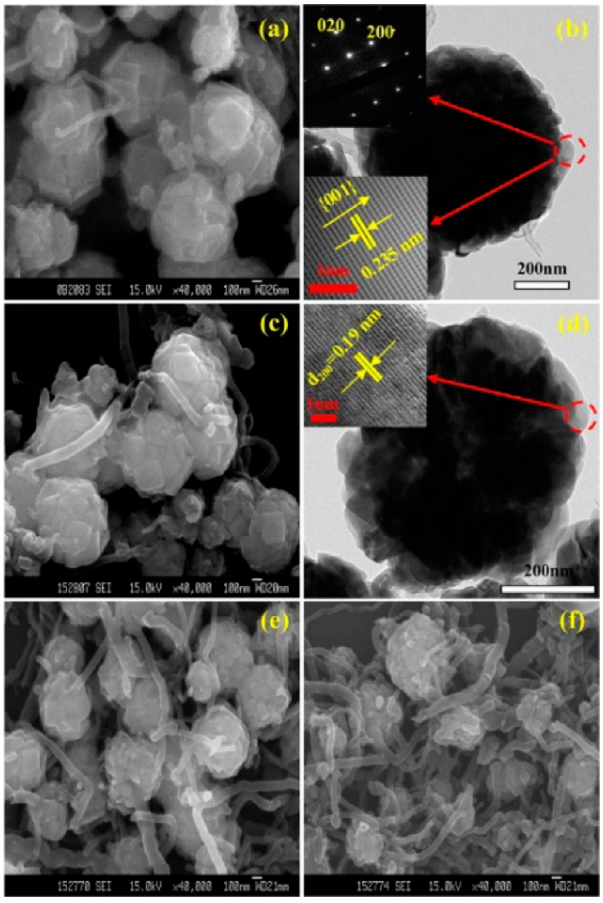


**Figure 2.** Scanning electron microscopy (SEM) and transmission electron microscopy (TEM) images of composite photocatalysts prepared with different MWCNT contents: (a and b) 7.2 wt %, (c and d) 18.9 wt %, (e) 31.7 wt %, and (f) 48.2 wt %. $TiO_2$ contents, from 92.8 to 51.8 wt %; hydrothermal temperature, 150 °C; and hydrothermal time, 72 h.[23]

simple liquid-phase deposition method using titanium tetrafluoride and electron beam (EB) irradiation-pretreated graphene as raw materials. The key synthesis parameters include graphene content, concentration of $TiF_4$ solution, and EB irradiation. A chemically bonded $TiO_2$ (P25)−graphene nanocomposite photocatalyst was prepared by a facile one-step hydrothermal method, in which simultaneous reduction of GO and loading of P25 was achieved.[16] Liu et al.[17] compared photocatalytic activities of graphene−$TiO_2$ systems from titanium isopropoxide and P25 and found that the $TiO_2$ precursor influenced the performance. Hydrothermal synthesis was also used to prepare graphene−$TiO_2$ nanotube (TNT) composites with enhanced photocatalytic activity. An alkaline hydrothermal process can convert $TiO_2$ nanoparticles to small-diameter TNTs on the reduced graphene oxide (rGO).[27] Using a hydrothermal method, graphene−$TiO_2$ nanowire was also prepared. GO reduction to graphene and hybridization between $TiO_2$ nanowires and graphene by forming a chemical bonding were achieved at a hydrothermal condition of 120 °C for 3 h.[28] In addition, robust hollow spheres of $Ti_{0.91}O_2$ nanosheets and graphene nanosheets were prepared by a layer-by-layer assembly method, shown in Figure 3.[29] The polymer beads were used as sacrificial templates, and a microwave irradiation technique was applied to simultaneously remove the template and reduce GO to graphene.

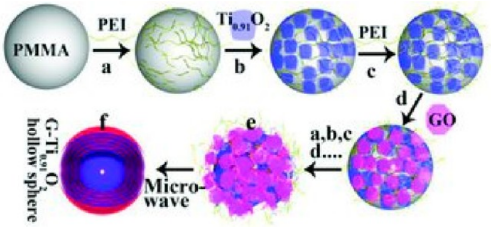


**Figure 3.** Layer-by-layer assembly preparation of hollow spheres of $Ti_{0.91}O_2$ nanosheets and graphene nanosheets.[29]

**2.2. Nanocarbon−ZnO Hybrids.** ZnO is another important photocatalyst, and it shows competitive catalytic performance to $TiO_2$.[30] Similar to nanocarbon−$TiO_2$ composites, various nanostructured carbon−ZnO hybrids were also prepared and tested for photocatalysis. MWCNT/ZnO composites can be prepared by a thermal hydrolysis method with MWCNT and zinc nitrate as precursors. The size of ZnO nanoparticles on the surface of the MWCNTs was about 18 nm.[31] ZnO−CNT can also be prepared under mild hydrothermal conditions ($T$ = 150−240 °C) with an autogenous pressure. CNTs are used as substrates for the growth of ZnO crystallites, and the crystallization of ZnO and its binding with CNTs take place simultaneously.[32] It was reported that MWCNT-supported metal-doped ZnO nanoparticles can be prepared in a simple and versatile approach by means of the co-deposition method. Mn, Mg, and Co salts are thus used and heat-treated at 450 °C, and MWCNTs can be modified by metal-doped nanoparticles.[33]

Graphene−ZnO nanoparticle hybrids were prepared by *in situ* thermal decomposition.[34] A single precursor, zinc benzoate dihydrazinate complex, can be thermally decomposed to form ZnO nanoparticles onto graphene at a low temperature of 200 °C. This method is simple and economical, with the product of uniform particle size, high yield, and no residual impurities. Liu et al.[35] reported the preparation of functionalized graphene sheet (FGS)/ZnO nanocomposites via a thermal treatment method. GO was used as a precursor of graphene; $Zn(NH_3)_4CO_3$ was used as a precursor of zinc oxide; and poly(vinyl pyrrolidone) was used as an intermediate to combine zinc with carbon materials. rGO−hierarchical ZnO hollow sphere composites were prepared by a simple ultrasonic method.[36] In the preparation, a mixed solution of GO, $Zn(CH_3COO)_2$, and dimethyl sulfoxide was ultrasonically treated for 15 min under ambient conditions. During the ultrasonic process, GO was reduced and ZnO hollow spheres were produced and loaded onto graphene sheets. Very recently, graphene−ZnO composites were also prepared using one-pot Zn powder and GO with or without a surfactant.[37] The photocatalyst presented higher activity than that prepared by $ZnCl_2$.

**2.3. Nanocarbon−Metal Sulfide Hybrids.** Some metal sulfides were found to be good photocatalysts with lower band gap energies than $TiO_2$ and ZnO and used for photocatalysis.[38,39] Microwave irradiation is a promising route for fabrication of nanocrystals, owing to the unique reaction effects, such as rapid volumetric heating, consequent dramatic increase in the reaction rate, etc. MWCNTs wrapped with face-centered cubic ZnS nanospheres with a uniform and small diameter have been prepared to create MWCNT/ZnS heterostructures by microwave irradiation.[40] The surfaces of MWCNTs are not only randomly decorated with ZnS layers, which were made of uniformed ZnS nanoparticles, but show some spherical particles


dx.doi.org/10.1021/ef401426x | *Energy Fuels* 2014, 28, 22−36

that aggregate and deposit on the layer. Cadmium sulfide (CdS) nanoparticles dotted on the surface of MWCNTs were synthesized by a polyol method. It was found that the nanosized CdS crystals are homogeneously dotted on the surfaces of MWCNTs, and the size of CdS decreases with an increasing concentration of MWCNTs in the samples.[41] CdS and $Ag_2S$ quantum dots (QDs) were deposited on poly(amidoamine) (PAMAM)-functionalized MWCNTs, in which the PAMAM macromolecules grown on MWCNTs were used as a platform for the deposition of the QDs. A series of novel and efficient visible-light-driven CNT/$Cd_{0.1}Zn_{0.9}S$ composite photocatalysts with low loading amount (0−1.0 wt %) of CNT were prepared by a simple one-pot hydrothermal method. Acid-treated CNT, $Zn(Ac)_2{\cdot}2H_2O$, and $Cd(Ac)_2{\cdot}2H_2O$ were used as precursors and treated by a hydrothermal process of 160 °C for 8 h.[42]

CdS-cluster-decorated graphene nanosheets were prepared by a solvothermal method, in which GO served as the support and cadmium acetate served as the CdS precursor. Nanosheets in the composite would increase the crystallinity and the specific surface area (SSA) of CdS clusters.[43] A hydrothermal method was employed to prepare a limited-layered $MoS_2$ co-catalyst confined on graphene sheets.[44] Two-dimensional (2D) rGO sheets not only provide a confined substrate for selective growth of limited-layered $MoS_2$ but also produce the interconnected 2D conductive frameworks for more efficient carriers transferring. Novel $In_2S_3$ nanosheet/graphene photocatalysts were also prepared by a cysteine-assisted one-pot hydrothermal method.[45] Cysteine, with multifunctional groups, can act as a sulfide source for the growth of $In_2S_3$ and as a reducing agent for GO reduction.

**2.4. Nanocarbon−Metal Hybrids.** Some nanosized metals, such as Ag and Au, show plasmonic effect and have been used for enhanced photocatalysis.[46] MWCNTs with polyoxometalate-encapsulated gold nanoparticles (Au NPs@POP−CNTs) were prepared by a green, facile one-pot synthesis method.[47] Figure 4 shows the preparation procedure. The polyoxometalates were used as both reducing and bridging molecules and avoided introducing other organic toxic molecules. The CNTs are endless with a rather smooth surface, and the diameters of the CNTs are several tens of nanometers. Well-dispersed Au NPs decorate the walls in an ordered manner. MWCNT-supported Ag nanoparticles (Ag/MWCNTs) were prepared by two methods (direct photoreduction and thermal decomposition). The samples from the thermal decompositions showed better performance in photocatalysis than those from photoreduction.[48]

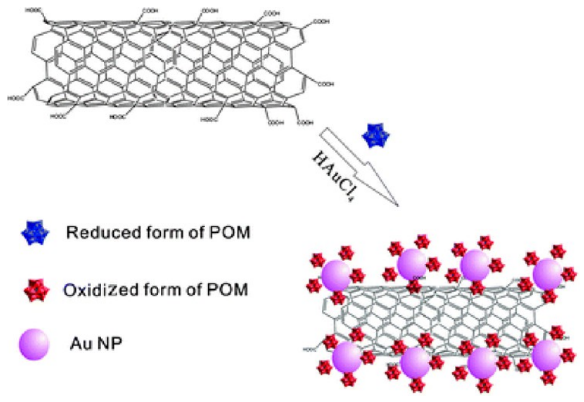


**Figure 4.** Preparation procedure of Au NPs@POP−CNTs.[47]

Zhao et al.[49] reported a preparation of graphene−gold nanocomposites as visible-light photocatalysts. GO was prepared by a modified Hummer's method, followed by a reduction using sodium borohydride with simultaneous reduction of chloroauric acid ($HAuCl_4$) onto rGO sheets.

**2.5. Metal-Free Nanocarbon Hybrids.** Very recently, nanocarbons themselves were found to be photocatalysts. GO from Hummer's method was demonstrated as a promising photocatalyst for $CO_2$ to methanol conversion.[20] Density functional theory (DFT) studies showed that both band gap and a working function of GO materials can be tuned to meet the requirement of the photocatalyst by varying the coverage and relative ratio of the surface groups.[50] A novel metal-free photocatalyst−sulfur/graphene (S/GR) composite was prepared by a facile two-step hydrothermal method with thiosulfate and GO as precursors. A green reductant of L-ascorbic acid was used to reduce GO to rGO under mild conditions.[51] Pillaring chemically exfoliated GO with CNTs was synthesized using the chemical vapor deposition (CVD) method with acetonitrile as the carbon source and nickel nanoparticles as the catalyst, as shown in Figure 5.[52] The amount and length of the CNT pillars connecting the rGO layers can be controlled by the amount of Ni catalyst and the reaction time of CVD.

Graphitic carbon nitride (g-$C_3N_4$) with a similar graphene structure was recently reported to show photocatalytic activity.[53,54] A GO-modified g-$C_3N_4$ hybrid was prepared by a sonochemical approach, in which a mixed solution of GO and g-$C_3N_4$ was ultrasonicated for 12 h and dried at 353 K for 12 h.[55] Graphene and g-$C_3N_4$ composite photocatalysts were also prepared by a combined impregnation−chemical reduction strategy. This preparation method includes polymerization of melamine in the presence of GO and hydrazine hydrate, followed by thermal treatment at 550 °C under nitrogen flow.[56] A novel MWCNT-modified white $C_3N_4$ composite (CNT/$C_3N_4$) with enhanced visible-light-response photoactivity was prepared by a hydrothermal method.[57] CNT and $C_3N_4$ were mixed in a

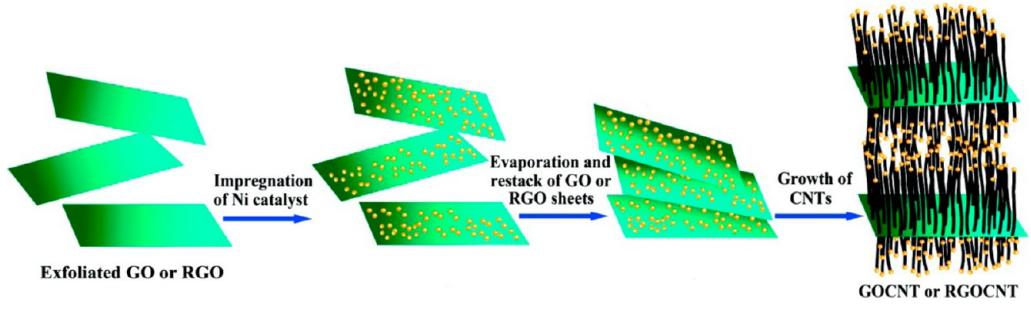


**Figure 5.** Procedure of pillaring GO and rGO with CNTs.[52]


dx.doi.org/10.1021/ef401426x | Energy Fuels 2014, 28, 22−36

**Table 1. Synthesis, Photocatalytic Performances, and Mechanisms of the Enhanced Activity of the Nanocarbon-Based Photocatalysts**

| photocatalyst | synthesis method | synthesis condition | photocatalytic application | mechanism of enhanced performance | reference |
|---|---|---|---|---|---|
| $TiO_2$/CNT | hydrolysis with ultrasonic irradiation | hydrolysis of titanium isopropoxide with CNTs ($TiO_2$/CNT: 1:01−0.2), followed by calcination at 400 °C | oxidation of acetone in air: activity is about 1.5 times higher than bare $TiO_2$ | lower $h^+/e^-$ recombination rate, higher BET, and more hydroxyl groups on the surface | 58 |
| MWCNT-supported $TiO_2$ | sol−gel or hydrothermal | $TiCl_4$ as the precursor and hydrothermal at 140 °C for 12 h; all samples annealed at 450 °C for 2 h | reduction of $CO_2$ with $H_2O$: overall $CO_2$ conversion is enhanced than bare $TiO_2$; sol−gel leads to formation of $C_2H_5OH$; and hydrothermal leads to production of HCOOH | mitigation of the agglomeration and decrease of the recombination rate of the $e^-/h^+$ pairs | 18 |
| CNT−$TiO_2$ | sol−gel | deposition of $TiO_2$ layers on CNT and then calcination under Ar at different temperatures | CNT−$TiO_2$ (70% $TiO_2$ + 30% CNT) shows the highest conversion and activity in propane oxidation | CNT (a) acts as a dispersing agent for producing a higher active surface area and (b) creates the CNT−$TiO_2$ interface for more efficient electron transfer | 59 |
| core−shell CNT−$TiO_2$ | surfactant wrapping sol−gel | organic Ti as precursors and NaDDBS as the surfactant, CNT/$TiO_2$ mass ratio of 0.9, and calcination at 500 °C for 30 min | CNT−$TiO_2$ shows higher photodegradation of methylene blue than bare $TiO_2$, and Ti-precursors affect the photocatalytic activity and photocurrent | reduction of the photoinduced electron/hole recombination rate | 22 |
| CNT−$TiO_2$ spheres | hydrothermal | titanium tetrafluoride as Ti precursor and CNTs as structure regulator; hydrothermal treatment and then calcination | degradation of gaseous styrene and decolorization of liquid-phase methyl orange | synergistic interaction between $TiO_2$ and MWCNTs | 23 |
| N-doped CNT−$TiO_2$ core−shell nanowires | biomimetic $TiO_2$ mineralization | $NH_3$ treatment of oxygenated CNTs and then coated by $TiO_2$ sol, followed by calcination | degradation of methylene blue and *p*-nitrophenol | band gap narrowing and higher BET surface area | 60 |
| $TiO_2$−graphene | liquid-phase deposition | titanium tetrafluoride and EB-irradiation-pretreated graphene as the raw materials | degradation of methyl orange: $TiO_2$−graphene shows much higher activity than their mixture | reduction of the $TiO_2$ crystal cluster size | 26 |
| $TiO_2$ nanotube−rGO | hydrothermal | decorating GO with $TiO_2$ nanoparticles, followed by an alkaline hydrothermal process of 120 °C for 24 h | degradation of malachite green oxalate: the composite shows an activity 3 times higher than pure CNT | effective charge transfer between CNT and graphene | 27 |
| $TiO_2$ nanowire−graphene | hydrothermal | mixing re-exfoliated GO with $TiO_2$ nanowires, followed by a hydrothermal process at 120 °C for 3 h | degradation of methylene blue: significant of graphene−$TiO_2$ composites than bare $TiO_2$ | enhanced adsorption and improved photogenerated electron/hole pairs separation | 28 |
| $Ti_{0.91}O_2$ nanosheet−graphene | layer-by-layer assembly | assembly with polymer beads as sacrificial templates using microwave irradiation to simultaneously remove the templates and reduce GO to rGO | photoreduction of $CO_2$ into CO and $CH_4$: the total yield conversion of $CO_2$ of the composites is 5 times higher than bare $Ti_{0.91}O_2$ | (a) fast movement of charge carriers, (b) enhanced lifetime of the charge carriers, and (c) enhanced light absorption | 29 |
| MWCNT−ZnO | thermal hydrolysis | addition of oxidized MWCNT to zinc nitrate and ammonia mixed solution, followed by drying and calcination at 300 °C | photodegradation of acetaldehyde: more than 40% higher in catalytic activity of MWCNT−ZnO than pure ZnO | higher BET surface area | 31 |
| graphene sheet−ZnO | thermal treatment | GO as a precursor of graphene, $Zn(NH_3)_4CO_3$ as a precursor of zinc oxide, and poly(vinyl pyrrolidone) as an intermediate to combine zinc with carbon materials, with calcination at 300 °C | photodegradation of rhodamine 6G: great improvement than pure ZnO | increased photon absorbance caused by graphene and electron transfer between ZnO and graphene | 35 |
| graphene-hybridized ZnO | simultaneous hybridization and reduction | exfoliated GO mixed with ZnO nanoparticles, followed by a reduction with hydrazine and ammonia | degradation of methylene blue: 5 times higher than pure ZnO | electronic interaction between graphene and ZnO | 61 |
| CdS−MWCNT | polyol | $Cd(CH_3COO)_2{\cdot}2H_2O$, thiourea, and MWCNT are mixed in diethylene glycol (DEG) and then heated at 180 °C for 2 h | photodegradation of Brilliant Red X-3B: higher activity of the MWCNT-supported CdS than CdS only | (a) improved ability to adsorb dye and $O_2$, (b) reduced recombination rate of the photogenerated electron/hole pairs, and (c) inhibited photocorrosion of CdS | 41 |
| CNT−$Cd_{0.1}Zn_{0.9}S$ composites | hydrothermal | acid-treated CNT, $Zn(Ac)_2{\cdot}2H_2O$, $Cd(Ac)_2{\cdot}2H_2O$, and thioacetamide were mixed and hydrothermally treated at 160 °C for 8 h | photocatalytic $H_2$ production: activity of the composite is 3.3 times higher than pure $Cd_{0.1}Zn_{0.9}S$ | CNTs can act as electron acceptors and transfer channels and enhance the charge separation efficiency | 42 |



dx.doi.org/10.1021/ef401426x | Energy Fuels 2014, 28, 22−36

**Table 1. continued**

| photocatalyst | synthesis method | synthesis condition | photocatalytic application | mechanism of enhanced performance | reference |
|---|---|---|---|---|---|
| CdS-cluster-decorated graphene nanosheets | solvothermal | GO and $Cd(Ac)_2{\cdot}2H_2O$ as precursors, dimethyl sulfoxide (DMSO) as solvent, solvothermal at 180 °C for 12 h | photocatalytic $H_2$ production: the composite shows about 4.69 times higher activity than pure CdS | (a) higher SSA and (b) graphene serves as an acceptor of the electrons and decreases the recombination rate of electron/hole pairs | 43 |
| rGO−$Cd_xZn_{1-x}S$ composites | co-precipitation−hydrothermal reduction | co-precipitation−hydrothermal in the presence of $Zn(Ac)_2{\cdot}2H_2O$, $Cd(Ac)_2{\cdot}2H_2O$, $Na_2S$, and GO; the weight ratios of GO/$Zn_{0.8}Cd_{0.2}S$ are 0, 0.1, 0.25, 0.5, 1, 2, and 5% | photocatalytic $H_2$ production: the composite shows about 4.5 times higher activity than pure $Zn_{0.8}Cd_{0.2}S$ | higher SSA and decreased recombination rate of electron/hole pairs | 62 |
| MWCNT with polyoxometalate-encapsulated gold nanoparticles | polyoxometalate (POM) reduction | POMs serve as both reducing, encapsulating molecules and bridging molecules and avoid introducing other toxic chemicals | photocatalytic degradation of rhodamine B: significant enhancement effects of the photocatalysis are observed on NPs@POM−CNT | enhanced separation rate of electron/hole pairs, increased BET, and good electrical conductivity | 47 |
| graphene−gold composite | chemical reduction | GO was prepared by modified Hummer's method, reduced using sodium borohydride, and then used for spontaneous chemical reduction of chloroauric acid | degradation of rhodamine B: the rate constant of GOR−Au was $8.7 \times 10^{-3}$ $min^{-1}$; the rate constant of P25−Au was $4.9 \times 10^{-3}$ $min^{-1}$; and the rate constant of GOR was $5.2 \times 10^{-4}$ $min^{-1}$ | (1) high adsorption ability, (2) strong $\pi-\pi$ interaction with dye chromophores, (3) efficient photosensitized electron injection, and (4) slow electron recombination | 49 |
| GO | modified Hummer's method | adjust the oxygenate group by excess $KMnO_4$ and $H_3PO_4$ | photocatalytic $CO_2$ reduction: $CO_2$ conversion rate of GO is 6-fold higher than the pure $TiO_2$ | modulated oxygenated functional groups | 20 |
| sulfur−graphene composite | hydrothermal | precipitation of sulfur from $Na_2S_2O_3{\cdot}5H_2O$ onto GO and then hydrothermal at 85 °C for 4 h | photodecomposition of methylene orange: about 5.9 times higher than pure sulfur | graphene can act as an electron collector and enhance the adsorption | 51 |
| CNT-pillared rGO composite | CVD | acetonitrile as the carbon source and nickel as the catalyst; CVD at 850 °C for 15−30 min | photocatalytic degradation of rhodamine B: 4 times faster than P25 | higher adsorption, strong $\pi-\pi$ interaction, efficient photosensitized electron injection, and decreased recombination rate | 52 |
| GO−g-$C_3N_4$ | sonochemical approach | GO from Hummer's method; g-$C_3N_4$ from directly heating melamine; and then their mixed solution is ultrasonicated for 12 h | degradation of RhB and 2,4-DCP: 3.80 times higher than pristine g-$C_3N_4$ | increased separation of the photoinduced carriers | 55 |



dx.doi.org/10.1021/ef401426x | Energy Fuels 2014, 28, 22−36

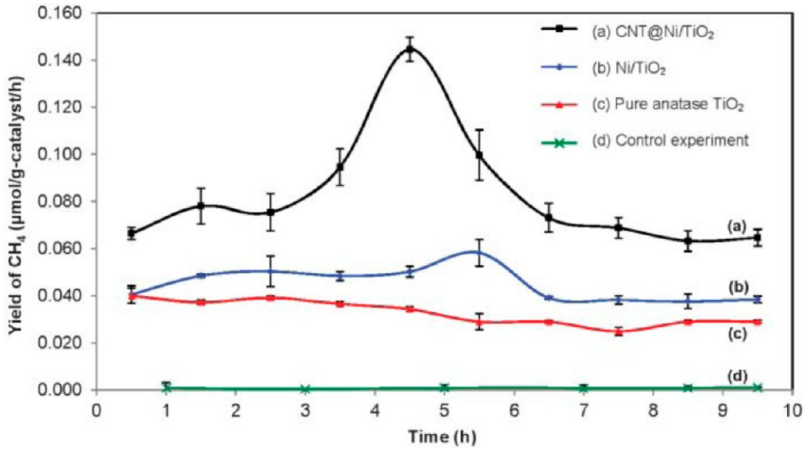


**Figure 6.** Time dependence upon the production rate of $CH_4$ over (a) CNT@Ni/$TiO_2$, (b) Ni/$TiO_2$, (c) pure anatase $TiO_2$, and (d) control experiment using CNT@Ni/$TiO_2$ without light irradiation.[64]

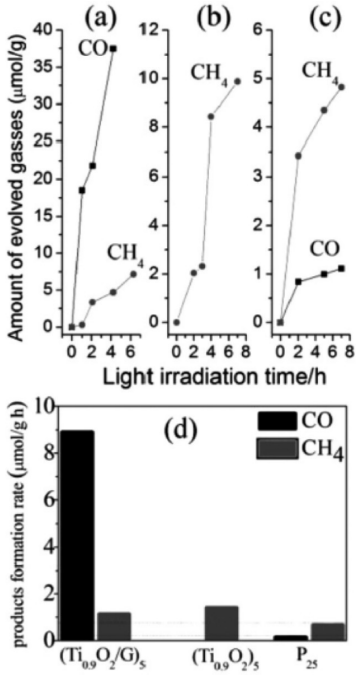


**Figure 7.** Photocatalytic $CO_2$ reduction to fuels: (a) $(G-Ti_{0.91}O_2)_5$ hollow spheres, (b) $(Ti_{0.91}O_2)_5$ hollow spheres, (c) P25, and (d) comparison of the average product formation rates.[29]

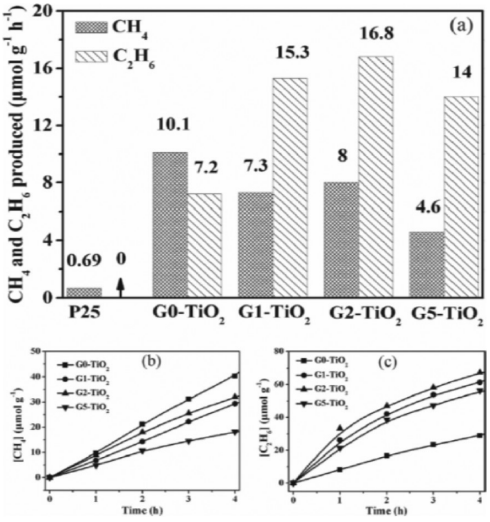


**Figure 8.** (a) Photoreduction of $CO_2$ on G$x$–$TiO_2$ ($x$ = 0, 1, 2, and 5) and P25. (b and c) Photocatalytic $CH_4$ and $C_2H_6$ evolution amounts for samples G$x$–$TiO_2$ ($x$ = 0, 1, 2, and 5).[65]

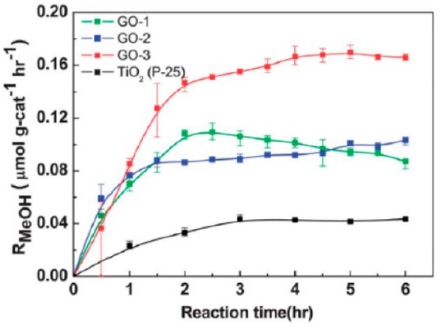


**Figure 9.** Photocatalytic $CO_2$ conversion to methanol over different photocatalysts.[20]

1-hexadecyl-3-methylimazolium chloride solution, followed by a hydrothermal process at 160 °C for 4 h.

Table 1 summarizes various nanocarbon-based photocatalysts, the synthesis method, and their enhanced photocatalytic performance in various applications. For synthesis, the hydrothermal method is simple and widely used. Other methods, such as solvothermal and thermal treatments as well as precipitation, are also employed.

## 3. PHOTOCATALYTIC $CO_2$ CONVERSION TO FUELS

**3.1. CNT-Based Photocatalysts.** There are a large number of studies addressing CNT hybrid photocatalysts for photodegradation of organic pollutants,[15,42,63] yet very limited reports were related to $CO_2$ reduction. MWCNT-supported anatase $TiO_2$ nanoparticles and rutile $TiO_2$ nanorods were prepared by sol–gel and hydrothermal methods, respectively, and their activities were examined in the reduction of $CO_2$ with $H_2O$.[18] A proper amount of MWCNTs in the composite can reduce the agglomeration of $TiO_2$ and effectively transport the photoinduced electron/hole pairs along the tubes, by which the recombination rate of carriers is decreased and the photocatalytic activity is enhanced. However, excessive MWCNTs would shield $TiO_2$ from absorbing UV, thus leading to less


dx.doi.org/10.1021/ef401426x | Energy Fuels 2014, 28, 22–36

**Table 2. Photocatalytic Reduction of $CO_2$ over Nanocarbon-Based Photocatalysts**

| catalyst | reaction condition | product | performance | nanocarbon function | reference |
|---|---|---|---|---|---|
| MWCNT-supported $TiO_2$ | $H_2O$ and $CO_2$ with a mole ratio of 5:1 and 15 W UV lamp with the wavelength of 365 nm as the irradiations | main formation of $C_2H_5OH$ from sample prepared by the sol–gel method and HCOOH from the sample prepared by the hydrothermal method, with a trance amount of $CH_4$ | highest total carbonaceous rate: 450.77 $\mu$mol/g | CNTs can mitigate the agglomeration of $TiO_2$ particles, transport the electron/hole pairs, and decrease the recombination rate of electron/hole pairs | 18 |
| CNT@Ni/$TiO_2$ | pure $CO_2$ flowing through a water bubbler and a low-power 75 W visible daylight lamp | $CH_4$ | highest $CH_4$ yield of 0.145 $\mu$mol $g^{-1}$ $h^{-1}$ | (a) synergistic combination of CNTs and $TiO_2$, (b) extended light absorption range and, (c) improved transportation of photogenerated charge carriers | 64 |
| graphene–titania composite | reduction in the presence of water, either under UV or visible light | $CH_4$ | 4.5 times more $CH_4$ than the P25 file under UV and 7.2 times higher than P25 under visible light | enhancing the electrical mobility | 19 |
| $Ti_{0.91}O_2$ and graphene composite | 0.01 g of catalyst in a 230 mL reactor, high-purity $CO_2$ gas, and 0.4 mL of water; 300 W xenon arc lamp as the light source | $CH_4$ and CO | major product of CO, 8.91 $\mu$mol $g^{-1}$ $h^{-1}$; $CH_4$, 1.14$\mu$mol $g^{-1}$ $h^{-1}$; overall conversion 5 times higher than pure $Ti_{0.91}O_2$ | faster separation of electron/hole pairs for higher activity and quick diffusion of electrons for selection of CO formation | 29 |
| $TiO_2$–graphene 2D sandwich-like hybrid | as above | $CH_4$ and $C_2H_6$ | highest total production at 8 $\mu$mol $g^{-1}$ $h^{-1}$ $CH_4$ and 16.8 $\mu$mol $g^{-1}$ $h^{-1}$ $C_2H_6$ | $\pi$ orbital of graphene matches well with the d orbital of $TiO_2$; chemical bond interactions and form d–$\pi$ electron overlap | 65 |
| graphene–$WO_3$ nanobelt composite | 0.1 g of catalyst in a 270 mL reactor (5.4 $cm^2$ window) and 1 mL of water flowed by $CO_2$ gas | $CH_4$ | $CH_4$ formation rate: 1.125 $\mu$mol $g^{-1}$ $h^{-1}$ | graphene can elevate the conduction band of $WO_3$ for hydrocarbon production | 66 |
| graphene-modified $NiO_x$–$Ta_2O_5$ | aerated $CO_2$ aqueous solution under UV–vis light irradiations from a 400 W metal halogen lamp | $CH_3OH$ and $H_2$ | 3.4 times more methanol than the sample without graphene | flat carbon can serve as a scaffold to (a) anchor $Ta_2O_5$, (b) improve charge separation and suppress the recombination, and (c) adsorb more $CO_2$ for methanol formation | 67 |
| GO | continuous gas flow reactor, 0.2 g of catalyst, and a 300 W commercial halogen lamp as the simulated solar source | methanol | methanol formation of 0.172 $\mu$mol $g^{-1}$ $h^{-1}$, 6-fold higher than pure $TiO_2$ | photocatalyst | 20 |



dx.doi.org/10.1021/ef401426x | Energy Fuels 2014, 28, 22–36

photoinduced carries for the $CO_2$ reduction. The differences in main products of $C_2H_5OH$ on anatase and HCOOH on rutile were observed and attributed to the varying crystal phases of titania. Chai et al.[64] prepared CNT@Ni/$TiO_2$ nanocomposites by co-precipitation followed by CVD. Figure 6 showed that the photocatalytic activity of $CO_2$ reduction follows the order CNT@Ni/$TiO_2$ > Ni/$TiO_2$ > $TiO_2$ under visible-light irradiations. CNT modification can improve the electronic structure of $TiO_2$ and lower the band gap energy to extend the visible-light absorption. A strong chemical interaction and improved intimate electrical contact between CNTs and $TiO_2$ were observed. The excited electrons from $TiO_2$ can transport to the conductive structure of CNTs, because they have a lower Fermi level via formation of a Schottky barrier at the interface. The heterojunction of CNTs and $TiO_2$ would also be beneficial to charge separation, stabilization, and hindered recombination.

**3.2. Graphene-Based Photocatalysts.** As a honeycomb-structured carbon sheet with $sp^2$ bonding, graphene has unique electronic properties, large theoretical SSA, and high transparency. All of these make graphene an excellent candidate for modifying a photocatalyst for enhanced photocatalytic performance.[16,36,49] The photocatalytic performance of the graphene hybrid photocatalysts were mostly tested in degradation of organic pollutants, and only in the last 3 years, some investigations on photocatalytic $CO_2$ conversion have been reported.

Graphene from rGO and solvent-exfoliated graphene (SEG) were employed by Hersam et al.[19] to prepared rGO−$TiO_2$ and SEG−$TiO_2$ photocatalysts. The 0.27 wt % SEG−P25 nanocomposite exhibited the highest photoreductive activity under UV, and its $CH_4$ production was 4.5 times higher than that on P25. On the other hand, 0.55 wt % SEG−P25 had the highest activity under visible light, with an enhancement at 7.2 times compared to pure P25. A direct correlation was found between the electrical mobility of the graphene component and the photocatalytic activity, indicating that graphene plays a significant role in photocatalytic reduction of $CO_2$.

Zhou et al.[29] prepared a $Ti_{0.91}O_2$ nanosheet and graphene nanosheet composite (G−$Ti_{0.91}O_2$) by a layer-by-layer assembly route. The photocatalytic activity of G−$Ti_{0.91}O_2$ hollow spheres was investigated by photocatalytic $CO_2$ conversion in the presence of water vapor, and the results are shown in Figure 7. It was found that CO was the major product with a small amount of $CH_4$ over G−$Ti_{0.91}O_2$. When using unmodified $Ti_{0.91}O_2$, $CH_4$ was the main product and no CO was detected. The overall $CO_2$ conversion on G−$Ti_{0.91}O_2$ was 5 times higher than $Ti_{0.91}O_2$ hollow spheres. The higher activity of G−$Ti_{0.91}O_2$ than $Ti_{0.91}O_2$ was attributed to the more efficient charge separation by the surface conjugation (d−$\pi$) of titania with graphene. CO formation is a two-electron transfer process, while $CH_4$ formation involves eight-electron transfer through the reaction route: $CO_2 \rightarrow CO \rightarrow C^{\bullet} \rightarrow CH_2 \rightarrow CH_4$. The introduction of graphene was beneficial for production of CO. The transferred electrons to graphene would diffuse very fast over the large area of carbon framework, increasing the electrical mobility of graphene. Therefore, the accumulation of the photoinduced electrons and local electron density are decreased; thus, two-electron reactions of CO formation are promoted.

$TiO_2$−graphene 2D sandwich-like hybrid nanosheets were prepared in a binary ethylenediamine (En)/$H_2O$ solvent.[65] Abundant $Ti^{3+}$ was detected on the surface of $TiO_2$ of the hybrid. $CH_4$ and $C_2H_6$ were produced by photoreduction of $CO_2$ over the prepared hybrid, and the results are shown in Figure 8. The total production rate increased with increasing graphene content. The d orbital of $TiO_2$ and $\pi$ orbital of graphene can match well in energy levels and then form a d−$\pi$ electron orbital overlap. Therefore, the photoinduced electrons from $TiO_2$ can transfer freely along the graphene network for $CO_2$ reduction, increasing the photocatalytic $CO_2$ conversion rate.

Bai et al.[66] demonstrated that graphene can elevate the conduction band of $WO_3$ for the photoreduction of $CO_2$ into hydrocarbon fuels under visible-light irradiations. $CH_4$ was the main product with detectable $CH_3OH$, $H_2$, and CO as secondary products. Without graphene, $TiO_2$ and $WO_3$ did not show activity in methane production. In addition, the graphene-modified $NiO_x$−$Ta_2O_5$ composite was prepared and used for the photocatalytic reduction of an aqueous $CO_2$ solution to $CH_3OH$ and $H_2$.[67] $NiO_x$−$Ta_2O_5$−rG containing 1% graphene showed the highest reduction of $CO_2$ to $CH_3OH$, producing 3.4 times more $CH_3OH$ than that on the counterpart without graphene.

**3.3. Metal-Free Hybrid Photocatalysts.** Metal-free carbonaceous materials of modified graphene,[51] graphene−CNT,[52] graphene−$C_3N_4$,[55] and CNT−$C_3N_4$[57] have demonstrated successfully degradation of organic pollutants in photocatalysis. As new composite materials, few investigations have been reported on their photocatalytic performance. More recently, photocatalytic $CO_2$ conversion to methanol was investigated over GO as a metal-free photocatalyst.[20] Figure 9 shows the photocatalytic methanol formation over GO-1 (Hummer's method), GO-2 (modified with 5 mL of $H_3PO_4$), GO-3 (modified with 10 mL of $H_3PO_4$), and $TiO_2$. Activity of methanol formation from photocatalytic $CO_2$ conversion followed the order: GO-3 > GO-1 > GO-2 > $TiO_2$ (P25). The photocatalytic $CO_2$ to methanol conversion rate of the modified GO-3 was 6 times higher than that of P25.

Some important results in photocatalytic conversion of $CO_2$ to solar fuels were summarized in Table 2, and the functions of different nanocarbon forms were illustrated. It is seen that major products of catalytic $CO_2$ reduction are $CH_4$ and $CH_3OH$. Nanocarbons can play various promoting roles in photocatalysis, which will be discussed below.

## 4. ROLES OF CNT AND GRAPHENE IN PHOTOCATALYTIC $CO_2$ CONVERSION

In comparison to photodegradation using nanocarbon-modified photocatalysts, photocatalytic $CO_2$ conversion over nanocarbon hybrids is quite a new field. However, available investigations have demonstrated the versatile roles of nanocarbons, especially CNTs and graphene, in photocatalytic $CO_2$ conversion to hydrocarbons. It has been found that nanocarbons in photocatalysts can reduce the band gap energy of semiconductors, separate photoinduced electron/hole pairs, increase reactant adsorption on the catalyst surface, and change redox potential, which will enhance catalytic activity and selectivity.

**4.1. Visible-Light Absorption and Band Gap Engineering.** The unique electronic properties of CNT facilitate its metallic or semiconducting features depending upon the geometry, therefore making it possible to produce cooperative or synergetic effects on a CNT−metal oxide hybrid.[68] It was found that the composites can absorb light at higher wavelengths than pure $TiO_2$; their absorption can be even extended to the whole range of the UV−vis spectrum. A correlation between the MWCNT content and UV−vis spectrum change was observed (Figure 10), and MWCNTs were found to work as a photosensitizer.[68] Liu et al.[69] reported that the visible-light absorption of MWCNT/$TiO_2$ was due to the new properties combining the features of MWCNTs and $TiO_2$. Zan et al.[70] suggested that MWCNT/$TiO_2$ would produce carbonaceous


dx.doi.org/10.1021/ef401426x | Energy Fuels 2014, 28, 22−36

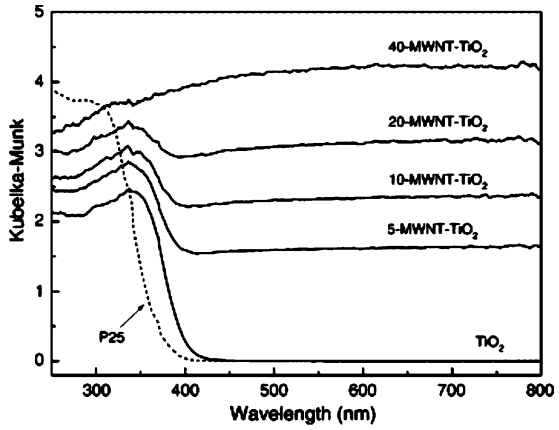


**Figure 10.** UV−vis spectra of $TiO_2$ with various contents (0, 5, 10, 20, and 40 wt %) of MWCNTs.[68]

Ti−C bonds on the interface between $TiO_2$ and MWCNTs, which enhanced the photoabsorbance of the hybrid materials in the visible-light region. Chai et al.[64] successfully demonstrated the visible-light photoreduction of $CO_2$ to methane by water under visible light on CNT@Ni/$TiO_2$. The band gap of the nanocomposites was 2.22 eV, as compared to that of 3.20 eV of a typical UV photocatalyst of $TiO_2$.

GO is an electronical hybrid material that can form a semiconductor by partial oxidation because of $\pi$ states from $sp^2$ carbon sites. It can also act as an insulator when fully oxidized and form a large energy gap (carrier transport gap) between $\sigma$ states of its $sp^3$-bonded carbons. The band gap energy can be tuned by the ratio of the $sp^2$ and $sp^3$ fractions with the varying contents of oxygen functional groups, therefore providing a flexible way to controllably transform GO from an insulator to a semiconductor and a graphene-like semi-metal.[71,72] Xu et al.[73] prepared graphene/$TiO_2$ nanosheet composites and found a wide background absorption in the visible-light region, which was attributed to the reduced reflection of light by the presence of carbon. In comparison to pure $TiO_2$, a red shift in the absorption edge and a strong absorption in the visible-light region on the hybrid materials could be observed. The visible-light response was attributed to the interaction between C and Ti atoms on the surface.[17,73]

Yang et al.[74] investigated the optical properties of graphene/ZnO nanocomposites using DFT calculations. Graphene was found to interact with ZnO via weak van der Waals interactions. The nanocomposites exhibited more effective UV absorption and enhanced visible-light response compared to ZnO. A red shift of the absorption threshold was as large as 1.0 eV (100 nm), because electrons could be directly excited from the valence band of graphene to the conduction band of ZnO.

Bai et al.[66] reported that graphene can elevate the conduction band (CB) of $WO_3$ toward photocatalytic reduction of $CO_2$ under visible-light irradiation. $WO_3$ has a band gap of ca. 2.7 eV for adsorption of visible light, but the rather low conduction band minimum (< −0.1 V versus NHE, pH 7) has limited its application of $CO_2$ conversion to hydrocarbon fuels. Figure 11 shows that the introduction of graphene to $WO_3$ will improve the visible-light absorption of $WO_3$ photocatalysts. $WO_3$ has a deeper valence band (VB) maximum of 0.37 eV than graphene/$WO_3$ (GW). Graphene can also elevate the CB minimum of the GW and make it higher than the redox potential of $CH_4/CO_2$ at −0.24 V. Such a band gap engineering by graphene makes

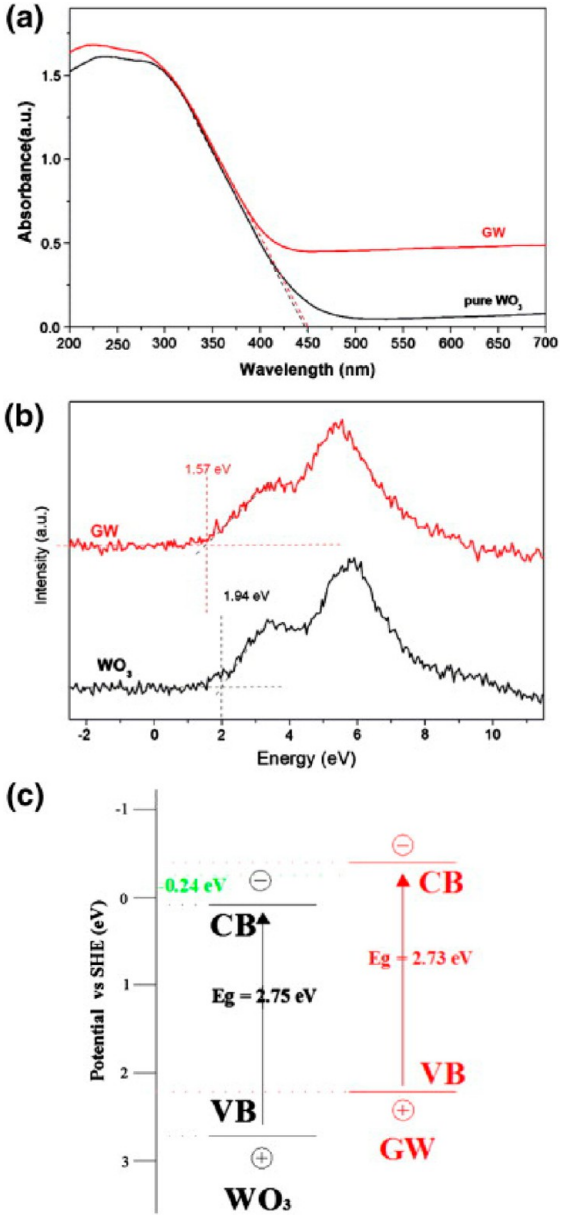


**Figure 11.** (a) UV−vis diffuse reflection spectra of pure $WO_3$ and GW, (b) X-ray photoelectron spectroscopy (XPS) VB spectra of pure $WO_3$ and GW, and (c) determined VB and CB edges of $WO_3$ and GW versus NHE (pH 7).[66]

the composites thermodynamically possible to reduce $CO_2$ by visible light.

**4.2. Electron/Hole Separation and Enhanced Photocatalytic Activity.** The enhanced photocatalytic activity by nanocarbon modification has been widely observed. Sigmund et al.[15] summarized two mechanisms of the enhancement of the photocatalytic properties of CNT−$TiO_2$ composites. The first mechanism suggested that the photoinduced electrons from $TiO_2$ can be transferred into CNTs and holes remain on the $TiO_2$ to conduct reactions. The second mechanism refers to the CNTs as sensitizers, which transfer electrons to the $TiO_2$. The electrons are injected into the conduction band of $TiO_2$, providing more electrons for surface reactions. Figure 12 proposes a schematic charge transfer of CNT/$TiO_2$ in $CO_2$ reduction with $H_2O$.[64] CNT can serve as a channel for electron storage to inhibit the recombination rate of electron/hole pairs.


dx.doi.org/10.1021/ef401426x | Energy Fuels 2014, 28, 22−36

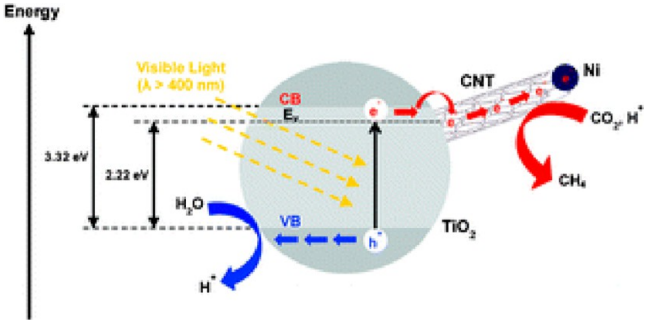


**Figure 12.** Schematic charge transfer for the photoreduction of $CO_2$ with $H_2O$ using CNT@Ni/$TiO_2$ nanocomposites.[64]

Moreover, long-range $\pi$-electronic conjugation of CNTs is beneficial in storing electrons, which can move freely along the walls of CNTs, leading to charge separation, stabilization, and hindered recombination.

Graphene has also been recognized as an electron collector and transporter to hinder electron/hole recombination and lengthen the electron/hole lifetime. Yao et al.[75] systematically investigated the mechanism for the enhanced photocatalytic activities of $TiO_2$/graphene using DFT calculations. The enhanced photocatalytic activity was ascribed to two processes: (a) graphene sheets significantly reduce the electron/hole recombination rate, and (b) excitation energy in the visible-light region for the VB maximum contributed from C 2p is far lower than Ti 3d.

Zhou et al.[65] discussed the mechanism of improved performance of $TiO_2$−graphene in $CO_2$ conversion. The produced electrons can conduct along the carbon network, and then the longer lifetime and mean free path for electrons on graphene will make the energetic electrons cover a larger area of the graphene surface and increase the likehood of the interaction with adsorbed reactants. Fu et al.[67] reported a tentative mechanism of photocatalytic reduction of $CO_2$ by $NiO_x$−$Ta_2O_5$−rGO, shown in Figure 13. Graphene serves as an electron collector and transporter to overcome the barrier of the recombination of charges to enhance the methanol production. Moreover, the unique features of graphene can allow for the photocatalytic reactions to take place not only on the surface of the photocatalyst but also on graphene sheets, largely enlarging the reaction space for enhanced activity.

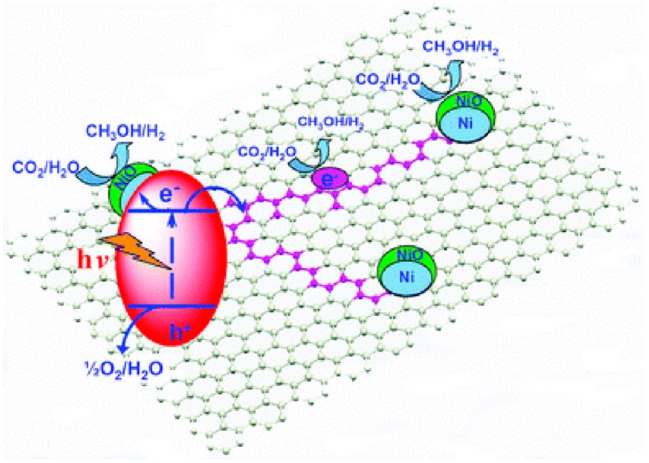


**Figure 13.** Charge separation and transfer in photoreduction of $CO_2$ on $NiO_x$−$Ta_2O_5$−rGO.[67]

**4.3. Improved Adsorption of Reactants.** Nanocarbons have demonstrated their large surface area and high activity/selectivity.[76] Graphene is a good sorbent candidate with a theoretical SSA of 2630 $m^2/g$; even rGO from chemically synthesized GO has a SSA at about 100 $m^2/g$.[77] Previous investigations have shown that CNTs and graphene exhibited high adsorption capacities in gas- and aqueous-phase adsorption.[78] Wang et al.[17] reported that graphene (G) in G/$TiO_2$ would increase the adsorption capacity of the photocatalysts. The reactant, methylene blue (MB) molecules, would transfer from the solution to the surface of the catalysts and be adsorbed with offset face-to-face orientation via $\pi$−$\pi$ conjugation between MB and aromatic regions of the graphene, leading to higher photocatalytic degradation efficiency. In photocatalytic $CO_2$ conversion, surface adsorption of $CO_2$ is also required. Rao et al.[79] reported that graphene samples prepared by exfoliation of GO or conversion of nanodiamond showed significant uptake of $CO_2$. $CO_2$ molecules would sit alternatively in a parallel fashion on the rings and showed a maximum uptake of 37.93 wt % in single-layer graphene.

**4.4. Tailored Selective Products.** Photocatalytic $CO_2$ conversion to hydrocarbons is a multiple-electron transfer system, and different hydrocarbons, such as $CH_4$, $CH_3OH$, CO, and HCOOH, can be produced. The modification of the photocatalysts will directly manipulate the generation and transfer of the photoinduced electron/hole pairs; therefore, the reactions listed in eqs 3−7 can be tuned. It was reported that, in the G−$Ti_{0.91}O_2$ system, CO was dominantly produced, while on pure $Ti_{0.91}O_2$, $CH_4$ is the main product.[29] The quick electron diffusion along the graphene sheet was suggested to be responsible for a better electronic mobility for a two-electron reaction of CO formation. Zhou et al.[65] also reported that the synergistic effect of the surface $Ti^{3+}$ sites and graphene favors the generation of $C_2H_6$ and the yield of $C_2H_6$ increases with the contents of the incorporated graphene.

**4.5. Traditional Photocatalysts and Drawbacks.** There are traditional alternatives to the nanocarbon-based photocatalysts in photoreduction of $CO_2$. $CO_2$ conversion under visible-light irradiations can be conducted on either modified wide-band semiconductors or low band gap photocatalysts. Zhang et al.[80] prepared copper and iodine co-modified $TiO_2$ nanoparticles and found that the materials can conduct photocatalytic reduction of $CO_2$ with water vapor to CO under visible light. Woolerton et al.[81] demonstrated that enzyme-modified $TiO_2$ nanoparticles can be used as photocatalysts for efficient and clean photoreduction of $CO_2$ to CO under visible light. Sato et al.[82] reported the successful development of a novel photocatalyst, mononuclear iridium(III) terpyridine (tpy) 2-phenylpyridine (ppy) complex, which showed selective reduction of $CO_2$ to CO under visible-light irradiations. Fujiwara et al.[83] reported the photocatalytic $CO_2$ reduction using quantized CdS nanocrystals. In comparison to nanocarbon-based photocatalysts, the modified $TiO_2$ requires complicated synthesis, and sometimes, the organic compounds would make the materials not stable. Some other low band gap visible-light photocatalysts, such as CdS or $WO_3$, suffer from high cost, poor stability, and toxicity to the environment.

Improving the separation rate of electron/hole pairs can significantly increase the photocatalytic activity in $CO_2$ photoreduction. Koci et al.[84] reported that modification of $TiO_2$ by silver can increase the yield of methane and methanol. At above


dx.doi.org/10.1021/ef401426x | Energy Fuels 2014, 28, 22−36

5% of Ag loading in $TiO_2$, Ag metallic clusters are formed in $TiO_2$ crystals with Shottky barrier at the metal−semiconductor interface, which spatially separates electrons and holes and decreases their recombination. Li et al.[85] found that the addition of Cu species can increase the overall $CO_2$ conversion efficiency by suppressing the electron/hole recombination. However, the stability of the Cu species was very low. In comparison to nanocarbons, silver is a noble metal with high cost and Cu is a transition metal with weak stability in the conditions of $CO_2$ reduction.

Improved adsorption of reactants is beneficial for the enhanced activity, which can be achieved at a higher Brunauer−Emmett−Teller (BET) surface area with good porous structure and proper surface property. Liu et al.[86] prepared a novel MgO-patched $TiO_2$ microsphere photocatalyst, which demonstrated 10 times higher activity toward CO production from $CO_2$ photoreduction with $H_2O$ vapor. The stable activity was attributed to the easier desorption of reaction intermediates and the enhanced $CO_2$ adsorption by MgO. Highly porous gallium oxide was synthesized by reconstructing its surface and bulk with meso- and macropores. The enhanced photocatalytic activity was mainly attributed to the 300% higher $CO_2$ adsorption capacity and the 200% increased surface area. The application of nanocarbons will use their unique structure and high BET surface area and avoid consuming metals and the tedious procedure for creating the porous structure.

Photoreduction of $CO_2$ to fuels involves many electron-transfer processes and various redox potentials; thus, the selectivity control is very difficult. Ikeue et al.[87] discovered that the differences in the $H_2O$ affinity to the zeolite surface led to a strong influence on the selectivity for the photocatalytic reduction of $CO_2$ with $H_2O$. Sato et al.[88] reported that selective reduction of $CO_2$ to formate over a p-type InP/Ru complex polymer hybrid can be highly enhanced by introduction of an anchoring complex into the polymer. In comparison to nanocarbons, the preparation of the zeolites and metal complex is complicated and expensive. Their stability in $CO_2$ conversion also requires improvement.

## 5. CONCLUSIVE REMARKS AND PERSPECTIVE

Barriers in future energy applications have been experienced in terms of shortage of fossil fuels and emission of greenhouse gas of carbon dioxide ($CO_2$). Using solar energy, photocatalytic conversion of $CO_2$ into hydrocarbons has demonstrated a promising strategy for sequestration of $CO_2$ to sustainable solar fuels. The efficiency of solar energy conversion to chemical fuels relies on the visible-light absorption, separation of photo-induced electron/hole carriers, and kinetics of surface reactions. The selectivity or preferred formation of certain chemicals can be tuned by the position of valence/conduction bands, which determines the redox potentials of the carriers. The key to control the activity and selectivity is the design of the photo-catalysts. Thus far, semiconductor photocatalysts, such as $TiO_2$, ZnO, CdS, GaN, $WO_3$, and SiC, have been applied in photo-reduction of $CO_2$, in which $TiO_2$ is the most popular material because of the high activity, non-toxicity, and low cost. Transition or noble metals and low band gap semiconductors have been used as sensitizers to improve the performance of large band gap semiconductors in photocatalytic $CO_2$ conversion.

It has been extensively proven that nanocarbon hybrid photocatalysts, such as $TiO_2$-, ZnO-, sulfide-, and metal-based materials, can be successfully prepared by a variety of methods. The photodegradation of organic pollutants were widely carried out over such nanocarbon-based photocatalysts; however, only a few reports using nanocarbon-based photocatalysts are available in the investigation of photocatalytic reduction of $CO_2$ to hydrocarbon fuels. Present studies show that graphene or CNT can play significant roles in the $CO_2$ conversion processes, such as improving visible-light absorption, activity enhancement, adsorption of reactants, improved selectivity, etc. Many future studies can be performed for the solar fuel production with simultaneous $CO_2$ sequestration using nanocarbons, such as screening available nanocarbon hybrid photocatalysts in photoreduction of $CO_2$, design of advanced nanocarbon-based photocatalysts, and theoretical investigations for $CO_2$ conversion on nanocarbons.

Thus far, the photocatalytic activity and selectivity in photocatalytic $CO_2$ conversion to hydrocarbon fuels are still far from practical application. Thermodynamic control of the photocatalysis, such as advanced photocatalyst material design for more excited carrier production and fast separation, needs to be investigated. As summarized, a great variety of nanocarbon-based photocatalysts have already been demonstrated to be effective in the degradation of organics in water/air and $H_2$ production. A comprehensive survey of these materials in photocatalytic $CO_2$ reduction would be helpful for finding effective photocatalysts. More complicated nanocarbon hybrid materials might be another solution, in which the surface functional groups and band structure are rationally designed. Different types of nanocarbons, such as nanospheres and QDs can be included. Moreover, the nature of nanocarbons, one-dimensional (1D) structure and semiconductor or metallic properties of CNTs, and 2D structure of GO and graphene and their surface functional groups should be correlated to the functions in photoreduction of $CO_2$. To this end, theoretical studies using DFT calculations are required to thoroughly illustrate the roles of nanocarbons in the photocatalysis. On the other hand, because a variety of products can be formed in the photocatalytic $CO_2$ conversion, a good selectivity to specific fuel is highly demanded for preventing the potential separation processes. Band gap engineering for preferential redox potentials of the photoinduced carriers can partially play the role. The diffuse and transfer of the photoinduced electrons can also be manipulated for improving the selectivity. At last, kinetic studies of the photocatalytic reactions, from surface charge transfer and interaction with reactants to desorption of the products, and reactor geometry are to be systematically investigated.

## AUTHOR INFORMATION

### Corresponding Authors

*E-mail: h.sun@curtin.edu.au.

*E-mail: shaobin.wang@curtin.edu.au.

### Notes

The authors declare no competing financial interest.

## ACKNOWLEDGMENTS

This research is financially supported by the Australian Research Council Discovery Projects (DP110103699 and DP130101319).

## REFERENCES

(1) Tran, P. D.; Wong, L. H.; Barber, J.; Loo, J. S. C. Recent advances in hybrid photocatalysts for solar fuel production. *Energy Environ. Sci.* **2012**, *5* (3), 5902−5918.

(2) Roy, S. C.; Varghese, O. K.; Paulose, M.; Grimes, C. A. Toward solar fuels: Photocatalytic conversion of carbon dioxide to hydrocarbons. *ACS Nano* **2010**, *4* (3), 1259−1278.
(3) Varghese, O. K.; Paulose, M.; LaTempa, T. J.; Grimes, C. A. High-rate solar photocatalytic conversion of $CO_2$ and water vapor to hydrocarbon fuels. *Nano Lett.* **2009**, *9* (2), 731−737.
(4) Inoue, T.; Fujishima, A.; Konishi, S.; Honda, K. Photoelectrocatalytic recuction of carbon-dioxide in aqueous suspensions of semiconductor powders. *Nature* **1979**, *277* (5698), 637−638.
(5) Liu, G. H.; Hoivik, N.; Wang, K. Y.; Jakobsen, H. Engineering $TiO_2$ nanomaterials for $CO_2$ conversion/solar fuels. *Sol. Energy Mater. Sol. Cells* **2012**, *105*, 53−68.
(6) Izumi, Y. Recent advances in the photocatalytic conversion of carbon dioxide to fuels with water and/or hydrogen using solar energy and beyond. *Coordin. Chem. Rev.* **2013**, *257* (1), 171−186.
(7) Tseng, I. H.; Chang, W. C.; Wu, J. C. S. Photoreduction of $CO_2$ using sol−gel derived titania and titania-supported copper catalysts. *Appl. Catal., B* **2002**, *37* (1), 37−48.
(8) Dzhabiev, T. S. Photoreduction of carbon dioxide with water in the presence of SiC/ZnO heterostructural semiconductor materials. *Kinet. Catal.* **1997**, *38* (6), 795−800.
(9) Barton, E. E.; Rampulla, D. M.; Bocarsly, A. B. Selective solar-driven reduction of $CO_2$ to methanol using a catalyzed p-GaP based photoelectrochemical cell. *J. Am. Chem. Soc.* **2008**, *130* (20), 6342−6343.
(10) Dhakshinamoorthy, A.; Navalon, S.; Corma, A.; Garcia, H. Photocatalytic $CO_2$ reduction by $TiO_2$ and related titanium containing solids. *Energy Environ. Sci.* **2012**, *5* (11), 9217−9233.
(11) Mori, K.; Yamashita, H.; Anpo, M. Photocatalytic reduction of $CO_2$ with $H_2O$ on various titanium oxide photocatalysts. *RSC Adv.* **2012**, *2* (8), 3165−3172.
(12) Navalon, S.; Dhakshinamoorthy, A.; Alvaro, M.; Garcia, H. Photocatalytic $CO_2$ reduction using non-titanium metal oxides and sulfides. *ChemSusChem* **2013**, *6* (4), 562−577.
(13) Meng, Z. D.; Zhu, L.; Choi, J. G.; Chen, M. L.; Oh, W. C. Effect of Pt treated fullerene/$TiO_2$ on the photocatalytic degradation of MO under visible light. *J. Mater. Chem.* **2011**, *21* (21), 7596−7603.
(14) Kim, K. D.; Dey, N. K.; Seo, H. O.; Kim, Y. D.; Lim, D. C.; Lee, M. Photocatalytic decomposition of toluene by nanodiamond-supported $TiO_2$ prepared using atomic layer deposition. *Appl. Catal., A* **2011**, *408* (1−2), 148−155.
(15) Woan, K.; Pyrgiotakis, G.; Sigmund, W. Photocatalytic carbon-nanotube−$TiO_2$ composites. *Adv. Mater.* **2009**, *21* (21), 2233−2239.
(16) Zhang, H.; Lv, X. J.; Li, Y. M.; Wang, Y.; Li, J. H. P25-graphene composite as a high performance photocatalyst. *ACS Nano* **2010**, *4* (1), 380−386.
(17) Liu, S. Z.; Sun, H. Q.; Liu, S. M.; Wang, S. B. Graphene facilitated visible light photodegradation of methylene blue over titanium dioxide photocatalysts. *Chem. Eng. J.* **2013**, *214*, 298−303.
(18) Xia, X. H.; Jia, Z. H.; Yu, Y.; Liang, Y.; Wang, Z.; Ma, L. L. Preparation of multi-walled carbon nanotube supported $TiO_2$ and its photocatalytic activity in the reduction of $CO_2$ with $H_2O$. *Carbon* **2007**, *45* (4), 717−721.
(19) Liang, Y. T.; Vijayan, B. K.; Gray, K. A.; Hersam, M. C. Minimizing graphene defects enhances titania nanocomposite-based photocatalytic reduction of $CO_2$ for improved solar fuel production. *Nano Lett.* **2011**, *11* (7), 2865−2870.
(20) Hsu, H. C.; Shown, I.; Wei, H. Y.; Chang, Y. C.; Du, H. Y.; Lin, Y. G.; Tseng, C. A.; Wang, C. H.; Chen, L. C.; Lin, Y. C.; Chen, K. H. Graphene oxide as a promising photocatalyst for $CO_2$ to methanol conversion. *Nanoscale* **2013**, *5* (1), 262−268.
(21) Fan, W. Q.; Zhang, Q. H.; Wang, Y. Semiconductor-based nanocomposites for photocatalytic $H_2$ production and $CO_2$ conversion. *Phys. Chem. Chem. Phys.* **2013**, *15* (8), 2632−2649.
(22) Li, Z.; Gao, B.; Chen, G. Z.; Mokaya, R.; Sotiropoulos, S.; Puma, G. L. Carbon nanotube/titanium dioxide (CNT/$TiO_2$) core−shell nanocomposites with tailored shell thickness, CNT content and photocatalytic/photoelectrocatalytic properties. *Appl. Catal., B* **2011**, *110*, 50−57.
(23) An, T. C.; Chen, J. Y.; Nie, X.; Li, G. Y.; Zhang, H. M.; Liu, X. L.; Zhao, H. J. Synthesis of carbon nanotube-anatase $TiO_2$ submicrometer-sized sphere composite photocatalyst for synergistic degradation of gaseous styrene. *ACS Appl. Mater. Interfaces* **2012**, *4* (11), 5988−5996.
(24) Cong, Y.; Li, X. K.; Qin, Y.; Dong, Z. J.; Yuan, G. M.; Cui, Z. W.; Lai, X. J. Carbon-doped $TiO_2$ coating on multiwalled carbon nanotubes with higher visible light photocatalytic activity. *Appl. Catal., B* **2011**, *107* (1−2), 128−134.
(25) Yu, Y.; Yu, J. C.; Chan, C. Y.; Che, Y. K.; Zhao, J. C.; Ding, L.; Ge, W. K.; Wong, P. K. Enhancement of adsorption and photocatalytic activity of $TiO_2$ by using carbon nanotubes for the treatment of azo dye. *Appl. Catal., B* **2005**, *61* (1−2), 1−11.
(26) Zhang, H. J.; Xu, P. P.; Du, G. D.; Chen, Z. W.; Oh, K.; Pan, D. Y.; Jiao, Z. A facile one-step synthesis of $TiO_2$/graphene composites for photodegradation of methyl orange. *Nano Res.* **2011**, *4* (3), 274−283.
(27) Perera, S. D.; Mariano, R. G.; Vu, K.; Nour, N.; Seitz, O.; Chabal, Y.; Balkus, K. J. Hydrothermal synthesis of graphene−$TiO_2$ nanotube composites with enhanced photocatalytic activity. *ACS Catal.* **2012**, *2* (6), 949−956.
(28) Pan, X.; Zhao, Y.; Liu, S.; Korzeniewski, C. L.; Wang, S.; Fan, Z. Y. Comparing graphene−$TiO_2$ nanowire and graphene−$TiO_2$ nanoparticle composite photocatalysts. *ACS Appl. Mater. Interfaces* **2012**, *4* (8), 3944−3950.
(29) Tu, W. G.; Zhou, Y.; Liu, Q.; Tian, Z. P.; Gao, J.; Chen, X. Y.; Zhang, H. T.; Liu, J. G.; Zou, Z. G. Robust hollow spheres consisting of alternating titania nanosheets and graphene nanosheets with high photocatalytic activity for $CO_2$ conversion into renewable fuels. *Adv. Funct. Mater.* **2012**, *22* (6), 1215−1221.
(30) Shukla, P.; Fatimah, I.; Wang, S.; Ang, H. M.; Tadé, M. O. Photocatalytic generation of sulphate and hydroxyl radicals using zinc oxide under low-power UV to oxidise phenolic contaminants in wastewater. *Catal. Today* **2010**, *157* (1−4), 410−414.
(31) Saleh, T. A.; Gondal, M. A.; Drmosh, Q. A.; Yamani, Z. H.; Al-yamani, A. Enhancement in photocatalytic activity for acetaldehyde removal by embedding ZnO nano particles on multiwall carbon nanotubes. *Chem. Eng. J.* **2011**, *166* (1), 407−412.
(32) Byrappa, K.; Dayananda, A. S.; Sajan, C. P.; Basavalingu, B.; Shayan, M. B.; Soga, K.; Yoshimura, M. Hydrothermal preparation of ZnO:CNT and $TiO_2$:CNT composites and their photocatalytic applications. *J. Mater. Sci.* **2008**, *43* (7), 2348−2355.
(33) Chen, C. S.; Liu, T. G.; Lin, L. W.; Xie, X. D.; Chen, X. H.; Liu, Q. C.; Liang, B.; Yu, W. W.; Qiu, C. Y. Multi-walled carbon nanotube-supported metal-doped ZnO nanoparticles and their photocatalytic property. *J. Nanopart. Res.* **2013**, *15* (1), 1295.
(34) Kavitha, T.; Gopalan, A. I.; Lee, K. P.; Park, S. Y. Glucose sensing, photocatalytic and antibacterial properties of graphene−ZnO nanoparticle hybrids. *Carbon* **2012**, *50* (8), 2994−3000.
(35) Yang, Y.; Ren, L. L.; Zhang, C.; Huang, S.; Liu, T. X. Facile fabrication of functionalized graphene sheets (FGS)/ZnO nanocomposites with photocatalytic property. *ACS Appl. Mater. Interfaces* **2011**, *3* (7), 2779−2785.
(36) Luo, Q. P.; Yu, X. Y.; Lei, B. X.; Chen, H. Y.; Kuang, D. B.; Su, C. Y. Reduced graphene oxide−hierarchical ZnO hollow sphere composites with enhanced photocurrent and photocatalytic activity. *J. Phys. Chem. C* **2012**, *116* (14), 8111−8117.
(37) Liu, S.; Sun, H.; Suvorova, A.; Wang, S. One-pot hydrothermal synthesis of ZnO-reduced graphene oxide composites using Zn powders for enhanced photocatalysis. *Chem. Eng. J.* **2013**, *229*, 533−539.
(38) Bao, N. Z.; Shen, L. M.; Takata, T.; Domen, K. Self-templated synthesis of nanoporous CdS nanostructures for highly efficient photocatalytic hydrogen production under visible. *Chem. Mater.* **2008**, *20* (1), 110−117.
(39) Hu, J. S.; Ren, L. L.; Guo, Y. G.; Liang, H. P.; Cao, A. M.; Wan, L. J.; Bai, C. L. Mass production and high photocatalytic activity of ZnS nanoporous nanoparticles. *Angew. Chem., Int. Ed.* **2005**, *44* (8), 1269−1273.

(40) Wu, H. Q.; Wang, Q. Y.; Yao, Y. Z.; Qian, C.; Zhang, X. J.; Wei, X. W. Microwave-assisted synthesis and photocatalytic properties of carbon nanotube/zinc sulfide heterostructures. *J. Phys. Chem. C* **2008**, *112* (43), 16779−16783.
(41) Ma, L. L.; Sun, H. Z.; Zhang, Y. G.; Lin, Y. L.; Li, J. L.; Yu, K. W. Y.; Yu, Y.; Tan, M.; Wang, J. B. Preparation, characterization and photocatalytic properties of CdS nanoparticles dotted on the surface of carbon nanotubes. *Nanotechnology* **2008**, *19* (11), 115709.
(42) Yu, J. G.; Yang, B.; Cheng, B. Noble-metal-free carbon nanotube−$Cd_{0.1}Zn_{0.9}S$ composites for high visible-light photocatalytic $H_2$-production performance. *Nanoscale* **2012**, *4* (8), 2670−2677.
(43) Li, Q.; Guo, B. D.; Yu, J. G.; Ran, J. R.; Zhang, B. H.; Yan, H. J.; Gong, J. R. Highly efficient visible-light-driven photocatalytic hydrogen production of CdS-cluster-decorated graphene nanosheets. *J. Am. Chem. Soc.* **2011**, *133* (28), 10878−10884.
(44) Min, S. X.; Lu, G. X. Sites for high efficient photocatalytic hydrogen evolution on a limited-layered $MoS_2$ cocatalyst confined on graphene sheets—The role of graphene. *J. Phys. Chem. C* **2012**, *116* (48), 25415−25424.
(45) An, X. Q.; Yu, J. C.; Wang, F.; Li, C. H.; Li, Y. C. One-pot synthesis of $In_2S_3$ nanosheets/graphene composites with enhanced visible-light photocatalytic activity. *Appl. Catal., B* **2013**, *129*, 80−88.
(46) Hou, W.; Cronin, S. B. A review of surface plasmon resonance-enhanced photocatalysis. *Adv. Funct. Mater.* **2013**, *23* (13), 1612−1619.
(47) Li, S. W.; Yu, X. L.; Zhang, G. J.; Ma, Y.; Yao, J. N.; Keita, B.; Louis, N.; Zhao, H. Green chemical decoration of multiwalled carbon nanotubes with polyoxometalate-encapsulated gold nanoparticles: Visible light photocatalytic activities. *J. Mater. Chem.* **2011**, *21* (7), 2282−2287.
(48) Yan, Y.; Sun, H. P.; Yao, P. P.; Kang, S. Z.; Mu, J. Effect of multi-walled carbon nanotubes loaded with Ag nanoparticles on the photocatalytic degradation of rhodamine B under visible light irradiation. *Appl. Surf. Sci.* **2011**, *257* (8), 3620−3626.
(49) Xiong, Z. G.; Zhang, L. L.; Ma, J. Z.; Zhao, X. S. Photocatalytic degradation of dyes over graphene−gold nanocomposites under visible light irradiation. *Chem. Commun.* **2010**, *46* (33), 6099−6101.
(50) Jiang, X.; Nisar, J.; Pathak, B.; Zhao, J. J.; Ahuja, R. Graphene oxide as a chemically tunable 2-D material for visible-light photocatalyst applications. *J. Catal.* **2013**, *299*, 204−209.
(51) Peng, W. C.; Li, X. Y. Synthesis of a sulfur−graphene composite as an enhanced metal-free photocatalyst. *Nano Res.* **2013**, *6* (4), 286−292.
(52) Zhang, L. L.; Xiong, Z. G.; Zhao, X. S. Pillaring chemically exfoliated graphene oxide with carbon nanotubes for photocatalytic degradation of dyes under visible light irradiation. *ACS Nano* **2010**, *4* (11), 7030−7036.
(53) Wang, Y.; Wang, X. C.; Antonietti, M. Polymeric graphitic carbon nitride as a heterogeneous organocatalyst: From photochemistry to multipurpose catalysis to sustainable chemistry. *Angew. Chem., Int. Ed.* **2012**, *51* (1), 68−89.
(54) Niu, P.; Zhang, L. L.; Liu, G.; Cheng, H. M. Graphene-like carbon nitride nanosheets for improved photocatalytic activities. *Adv. Funct. Mater.* **2012**, *22* (22), 4763−4770.
(55) Liao, G. Z.; Chen, S.; Quan, X.; Yu, H. T.; Zhao, H. M. Graphene oxide modified g-$C_3N_4$ hybrid with enhanced photocatalytic capability under visible light irradiation. *J. Mater. Chem.* **2012**, *22* (6), 2721−2726.
(56) Xiang, Q. J.; Yu, J. G.; Jaroniec, M. Preparation and enhanced visible-light photocatalytic $H_2$-production activity of graphene/$C_3N_4$ composites. *J. Phys. Chem. C* **2011**, *115* (15), 7355−7363.
(57) Xu, Y. G.; Xu, H.; Wang, L.; Yan, J.; Li, H. M.; Song, Y. H.; Huang, L. Y.; Cai, G. B. The CNT modified white $C_3N_4$ composite photocatalyst with enhanced visible-light response photoactivity. *Dalton Trans.* **2013**, *42* (21), 7604−7613.
(58) Yu, Y.; Yu, J. C.; Yu, J. G.; Kwok, Y. C.; Che, Y. K.; Zhao, J. C.; Ding, L.; Ge, W. K.; Wong, P. K. Enhancement of photocatalytic activity of mesoporous $TiO_2$ by using carbon nanotubes. *Appl. Catal., A* **2005**, *289* (2), 186−196.
(59) Bouazza, N.; Ouzzine, M.; Lillo-Rodenas, M. A.; Eder, D.; Linares-Solano, A. $TiO_2$ nanotubes and CNT−$TiO_2$ hybrid materials for the photocatalytic oxidation of propene at low concentration. *Appl. Catal., B* **2009**, *92* (3−4), 377−383.
(60) Lee, W. J.; Lee, J. M.; Kochuveedu, S. T.; Han, T. H.; Jeong, H. Y.; Park, M.; Yun, J. M.; Kwon, J.; No, K.; Kim, D. H.; Kim, S. O. Biomineralized N-doped CNT/$TiO_2$ core/shell nanowires for visible light photocatalysis. *ACS Nano* **2012**, *6* (1), 935−943.
(61) Xu, T. G.; Zhang, L. W.; Cheng, H. Y.; Zhu, Y. F. Significantly enhanced photocatalytic performance of ZnO via graphene hybridization and the mechanism study. *Appl. Catal., B* **2011**, *101* (3−4), 382−387.
(62) Zhang, J.; Yu, J. G.; Jaroniec, M.; Gong, J. R. Noble metal-free reduced graphene oxide−$Zn_xCd_{1-x}S$ nanocomposite with enhanced solar photocatalytic $H_2$-production performance. *Nano Lett.* **2012**, *12* (9), 4584−4589.
(63) Martinez, C.; Canle, M.; Fernandez, M. I.; Santaballa, J. A.; Faria, J. Kinetics and mechanism of aqueous degradation of carbamazepine by heterogeneous photocatalysis using nanocrystalline $TiO_2$, ZnO and multi-walled carbon nanotubes−anatase composites. *Appl. Catal., B* **2011**, *102* (3−4), 563−571.
(64) Ong, W. J.; Gui, M. M.; Chai, S. P.; Mohamed, A. R. Direct growth of carbon nanotubes on Ni/$TiO_2$ as next generation catalysts for photoreduction of $CO_2$ to methane by water under visible light irradiation. *RSC Adv.* **2013**, *3* (14), 4505−4509.
(65) Tu, W. G.; Zhou, Y.; Liu, Q.; Yan, S. C.; Bao, S. S.; Wang, X. Y.; Xiao, M.; Zou, Z. G. An in situ simultaneous reduction−hydrolysis technique for fabrication of $TiO_2$−graphene 2D sandwich-like hybrid nanosheets: Graphene-promoted selectivity of photocatalytic-driven hydrogenation and coupling of $CO_2$ into methane and ethane. *Adv. Funct. Mater.* **2013**, *23* (14), 1743−1749.
(66) Wang, P. Q.; Bai, Y.; Luo, P. Y.; Liu, J. Y. Graphene−$WO_3$ nanobelt composite: Elevated conduction band toward photocatalytic reduction of $CO_2$ into hydrocarbon fuels. *Catal. Commun.* **2013**, *38*, 82−85.
(67) Lv, X. J.; Fu, W. F.; Hu, C. Y.; Chen, Y.; Zhou, W. B. Photocatalytic reduction of $CO_2$ with $H_2O$ over a graphene-modified $NiO_x$−$Ta_2O_5$ composite photocatalyst: Coupling yields of methanol and hydrogen. *RSC Adv.* **2013**, *3* (6), 1753−1757.
(68) Wang, W. D.; Serp, P.; Kalck, P.; Faria, J. L. Visible light photodegradation of phenol on MWNT−$TiO_2$ composite catalysts prepared by a modified sol−gel method. *J. Mol. Catal. A: Chem.* **2005**, *235* (1−2), 194−199.
(69) An, G. M.; Ma, W. H.; Sun, Z. Y.; Liu, Z. M.; Han, B. X.; Miao, S. D.; Miao, Z. J.; Ding, K. L. Preparation of titania/carbon nanotube composites using supercritical ethanol and their photocatalytic activity for phenol degradation under visible light irradiation. *Carbon* **2007**, *45* (9), 1795−1801.
(70) Tian, L. H.; Ye, L. Q.; Deng, K. J.; Zan, L. $TiO_2$/carbon nanotube hybrid nanostructures: Solvothermal synthesis and their visible light photocatalytic activity. *J. Solid State Chem.* **2011**, *184* (6), 1465−1471.
(71) Eda, G.; Mattevi, C.; Yamaguchi, H.; Kim, H.; Chhowalla, M. Insulator to semimetal transition in graphene oxide. *J. Phys. Chem. C* **2009**, *113* (35), 15768−15771.
(72) Loh, K. P.; Bao, Q. L.; Eda, G.; Chhowalla, M. Graphene oxide as a chemically tunable platform for optical applications. *Nat. Chem.* **2010**, *2* (12), 1015−1024.
(73) Wang, W. S.; Wang, D. H.; Qu, W. G.; Lu, L. Q.; Xu, A. W. Large ultrathin anatase $TiO_2$ nanosheets with exposed {001} facets on graphene for enhanced visible light photocatalytic activity. *J. Phys. Chem. C* **2012**, *116* (37), 19893−19901.
(74) Hu, W.; Li, Z. Y.; Yang, J. L. Electronic and optical properties of graphene and graphitic ZnO nanocomposite structures. *J. Chem. Phys.* **2013**, *138* (12), 124706.
(75) Geng, W.; Liu, H. X.; Yao, X. J. Enhanced photocatalytic properties of titania−graphene nanocomposites: A density functional theory study. *Phys. Chem. Chem. Phys.* **2013**, *15* (16), 6025−6033.

(76) Sun, H. Q.; Liu, S. Z.; Zhou, G. L.; Ang, H. M.; Tade, M. O.; Wang, S. B. Reduced graphene oxide for catalytic oxidation of aqueous organic pollutants. *ACS Appl. Mater. Interfaces* **2012**, *4* (10), 5466−5471.
(77) Peng, W. C.; Liu, S. Z.; Sun, H. Q.; Yao, Y. J.; Zhi, L. J.; Wang, S. B. Synthesis of porous reduced graphene oxide as metal-free carbon for adsorption and catalytic oxidation of organics in water. *J. Mater. Chem. A* **2013**, *1* (19), 5854−5859.
(78) Wang, S.; Sun, H.; Ang, H. M.; Tadé, M. O. Adsorptive remediation of environmental pollutants using novel graphene-based nanomaterials. *Chem. Eng. J.* **2013**, *226* (0), 336−347.
(79) Ghosh, A.; Subrahmanyam, K. S.; Krishna, K. S.; Datta, S.; Govindaraj, A.; Pati, S. K.; Rao, C. N. R. Uptake of $H_2$ and $CO_2$ by graphene. *J. Phys. Chem. C* **2008**, *112* (40), 15704−15707.
(80) Zhang, Q. Y.; Gao, T. T.; Andino, J. M.; Li, Y. Copper and iodine co-modified $TiO_2$ nanoparticles for improved activity of $CO_2$ photoreduction with water vapor. *Appl. Catal., B* **2012**, *123*, 257−264.
(81) Woolerton, T. W.; Sheard, S.; Reisner, E.; Pierce, E.; Ragsdale, S. W.; Armstrong, F. A. Efficient and clean photoreduction of $CO_2$ to CO by enzyme-modified $TiO_2$ nanoparticles using visible light. *J. Am. Chem. Soc.* **2010**, *132* (7), 2132−2133.
(82) Sato, S.; Morikawa, T.; Kajino, T.; Ishitani, O. A highly efficient mononuclear iridium complex photocatalyst for $CO_2$ reduction under visible light. *Angew. Chem., Int. Ed.* **2013**, *52* (3), 988−992.
(83) Fujiwara, H.; Hosokawa, H.; Murakoshi, K.; Wada, Y.; Yanagida, S.; Okada, T.; Kobayashi, H. Effect of surface structures on photocatalytic $CO_2$ reduction using quantized CdS nanocrystallites. *J. Phys. Chem. B* **1997**, *101* (41), 8270−8278.
(84) Koci, K.; Mateju, K.; Obalova, L.; Krejcikova, S.; Lacny, Z.; Placha, D.; Capek, L.; Hospodkova, A.; Solcova, O. Effect of silver doping on the $TiO_2$ for photocatalytic reduction of $CO_2$. *Appl. Catal., B* **2010**, *96* (3−4), 239−244.
(85) Li, Y.; Wang, W. N.; Zhan, Z. L.; Woo, M. H.; Wu, C. Y.; Biswas, P. Photocatalytic reduction of $CO_2$ with $H_2O$ on mesoporous silica supported Cu/$TiO_2$ catalysts. *Appl. Catal., B* **2010**, *100* (1−2), 386−392.
(86) Liu, L. J.; Zhao, C. Y.; Zhao, H. L.; Pitts, D.; Li, Y. Porous microspheres of MgO-patched $TiO_2$ for $CO_2$ photoreduction with $H_2O$ vapor: Temperature-dependent activity and stability. *Chem. Commun.* **2013**, *49* (35), 3664−3666.
(87) Ikeue, K.; Yamashita, H.; Anpo, M.; Takewaki, T. Photocatalytic reduction of $CO_2$ with $H_2O$ on Ti−$\beta$ zeolite photocatalysts: Effect of the hydrophobic and hydrophilic properties. *J. Phys. Chem. B* **2001**, *105* (35), 8350−8355.
(88) Sato, S.; Arai, T.; Morikawa, T.; Uemura, K.; Suzuki, T. M.; Tanaka, H.; Kajino, T. Selective $CO_2$ conversion to formate conjugated with $H_2O$ oxidation utilizing semiconductor/complex hybrid photocatalysts. *J. Am. Chem. Soc.* **2011**, *133* (39), 15240−15243.